

Combinatorial Level Densities from a Relativistic Structure Model

R. Pezer^a

^a*Physics Department, Faculty of Science, University of Zagreb, Croatia*

A. Ventura^{b,1,*}

^b *Ente Nuove Tecnologie, Energia e Ambiente, Bologna, Italy*
and Istituto Nazionale di Fisica Nucleare, Sezione di Bologna, Italy

D. Vretenar^c

^c*Physics Department, Faculty of Science, University of Zagreb, Croatia*

Abstract

A new model for calculating nuclear level densities is investigated. The single-nucleon spectra are calculated in a relativistic mean-field model with energy-dependent effective mass, which yields a realistic density of single-particle states at the Fermi energy. These microscopic single-nucleon states are used in a fast combinatorial algorithm for calculating the non-collective excitations of nuclei. The method, when applied to magic and semi-magic nuclei, such as ^{60}Ni , ^{114}Sn and ^{208}Pb , reproduces the cumulative number of experimental states at low excitation energy, as well as the *s*-wave neutron resonance spacing at the neutron binding energy. Experimental level densities above 10 MeV are reproduced by multiplying the non-collective level densities by a simple vibrational enhancement factor. Problems to be solved in the extension to open-shell nuclei are discussed.

Key words: Nuclear level densities, self-consistent relativistic models, combinatorial methods, vibrational enhancement

PACS: 21.10.Ma, 21.60.Jz

* Corresponding author.

Email address: ventura@bologna.enea.it (A. Ventura).

¹ Address: ENEA - Via Martiri di Monte Sole 4 - 40129 Bologna, Italy.

1 Introduction

Nuclear level densities have been a lively field of research for over sixty years since the pioneering work of Bethe[1]. The subject is interesting both from a purely theoretical point of view (the problem of a quantum many-body system with continuum excitation energy), as well as from a perspective of applications (e.g. an essential ingredient of statistical models of nuclear reactions).

Owing to their computational simplicity, phenomenological formulae for nuclear level densities with parameters adjusted to empirical data available at low excitation energy (cumulative numbers of discrete levels and s-wave neutron resonance spacings), have been used for many years. Their extrapolation to those regions of the periodic chart where there is no experimental information is, however, doubtful. The calculation of nuclear level densities should be rather based on microscopic structure models, and should make use of fast computational algorithms in order to deal with huge numbers of states that increase exponentially with excitation energy [1].

In this work we investigate a new model for calculating nuclear level densities. The method combines an efficient combinatorial algorithm based on the Gaussian polynomial expansion of a generating function [2], and an improved relativistic mean-field structure model with energy-dependent effective mass [3]. The microscopic structure model not only reproduces the bulk nuclear properties over the whole periodic chart, but it also yields realistic densities of single-nucleon states around the Fermi energy, an essential requirement for a self-consistent mean-field approach to nuclear level densities.

In Section 2 we outline the relativistic mean-field model with energy-dependent effective mass. The combinatorial algorithm for calculating nuclear level densities is described in Section 3. In this work applications are limited to magic and semi-magic nuclei. Empirical data at excitation energies above 10 MeV can be reproduced at the price of introducing a vibrational enhancement factor, described in Section 4. Our numerical results are compared with experimental data in Section 5. In Sec. 6 we summarize the results and present an outlook for future applications.

2 Relativistic Structure Model

The microscopic nuclear structure model adopted in the present work is described in detail in Ref. [3], where it has also been applied in the calculation of single-nucleon states in magic nuclei, e.g. ^{132}Sn and ^{208}Pb . In order to make the present analysis self-contained, the essential features of the model are

summarized in this section. Here and in the following, use is made of units $\hbar = c = 1$.

In the relativistic mean-field approximation [4], nucleons are described as point particles that move independently in mean fields which originate from the nucleon-nucleon interaction. The theory is fully Lorentz invariant. Conditions of causality and Lorentz invariance impose that the interaction is mediated by the exchange of point-like effective mesons, which couple to the nucleons at local vertices. The single-nucleon dynamics is described by the Dirac equation

$$\left\{ -i\boldsymbol{\alpha} \cdot \boldsymbol{\nabla} + \beta(m + g_\sigma \sigma) + g_\omega \omega^0 + g_\rho \tau_3 \rho_3^0 + e \frac{(1 - \tau_3)}{2} A^0 \right\} \psi_i = \varepsilon_i \psi_i. \quad (1)$$

σ , ω , and ρ are the meson fields, and A denotes the electromagnetic potential. g_σ , g_ω , and g_ρ are the corresponding coupling constants for the mesons to the nucleon. The lowest order of the quantum field theory is the *mean-field* approximation: the meson field operators are replaced by their expectation values. The sources of the meson fields are defined by the nucleon densities and currents. The ground state of a nucleus is described by the stationary self-consistent solution of the coupled system of the Dirac (1) and Klein-Gordon equations:

$$[-\Delta + m_\sigma^2] \sigma(\mathbf{r}) = -g_\sigma \rho_s(\mathbf{r}) - g_2 \sigma^2(\mathbf{r}) - g_3 \sigma^3(\mathbf{r}) \quad (2)$$

$$[-\Delta + m_\omega^2] \omega^0(\mathbf{r}) = g_\omega \rho_v(\mathbf{r}) \quad (3)$$

$$[-\Delta + m_\rho^2] \rho^0(\mathbf{r}) = g_\rho \rho_3(\mathbf{r}) \quad (4)$$

$$-\Delta A^0(\mathbf{r}) = e \rho_p(\mathbf{r}), \quad (5)$$

for the sigma meson, omega meson, rho meson and photon field, respectively. Due to charge conservation, only the 3rd-component of the isovector $\vec{\rho}$ meson contributes. The source terms in equations (2) to (5) are sums of bilinear products of baryon amplitudes, and they are calculated in the *no-sea* approximation, i.e. the Dirac sea of negative energy states does not contribute to the nucleon densities and currents. Due to time reversal invariance, there are no currents in the static solution for an even-even system, and therefore the spatial vector components ω , ρ_3 and \mathbf{A} of the vector meson fields vanish. The quartic potential

$$U(\sigma) = \frac{1}{2} m_\sigma^2 \sigma^2 + \frac{1}{3} g_2 \sigma^3 + \frac{1}{4} g_3 \sigma^4 \quad (6)$$

introduces an effective density dependence. The non-linear self-interaction of the σ field is essential for a quantitative description of properties of finite nuclei.

The effective single-nucleon potential is essentially given by the sum of the scalar attractive σ -potential and the vector repulsive ω -potential. Both potentials are of the order of several hundred MeV in the nuclear interior. The contributions of the isovector ρ -meson field and the electromagnetic interaction are much smaller. In the relativistic Hartree mean-field approximation the nucleon self-energy is real, local and energy independent. However, due to the momentum dependence of the scalar density or, equivalently, the momentum dependence of the Dirac mass in the non-relativistic reduction of the Dirac equation, even in the Hartree approximation the equivalent Schrödinger potential is nonlocal, i.e. momentum dependent[3].

In applications of the standard relativistic mean-field model to the description of ground state properties of spherical and deformed nuclei, the approximation of the real, local and energy independent nucleon self-energy leads to the well known problem of low effective mass, i.e. low density of single-nucleon states close to the Fermi surface. The problem of defining, in the relativistic framework, a local energy-dependent potential equivalent to a microscopic non-local potential, was discussed in detail in Ref. [5]. In a subsequent article [6] the same authors applied the relativistic Brückner-Hartree-Fock approximation to the calculation of dispersion relations that connect the real and imaginary parts of the Lorentz components of the mean field in symmetric nuclear matter and showed, in particular, that the total dispersive contribution to the real part of the mean field depends almost linearly on energy in an interval of half-width 10 MeV around the Fermi energy E_F .

The effect of non-locality in space and time of the underlying microscopic potential on the equivalent local and energy dependent potential in a relativistic theory, is conveniently expressed in terms of an effective nucleon mass m^* . The effective mass should not to be confused, however, with the Dirac mass, $m_D = m + g_\sigma \sigma$, appearing in Eq. (1). The latter is always smaller than m , due to the fact that $g_\sigma \sigma$ is an attractive potential, of the order of $0.5m$ in the nuclear interior, and very close to m at the surface, where σ goes to zero. As shown in detail in Refs.[5,6], the effective mass which is directly connected with the density of single particle states around the Fermi energy E_F , i.e. the crucial parameter of any nuclear state density model, can be defined as follows:

$$\frac{m^*(E)}{m} = 1 - \frac{dV_e(E)}{dE}, \quad (7)$$

where $E = \varepsilon - m$ is the difference between the total nucleon energy, ε , and its rest mass, and $V_e(E)$ is the real part of the energy-dependent Schrödinger-equivalent potential. In symmetric nuclear matter V_e reads [5]:

$$V_e(E) = V_\sigma + V_\omega + \frac{E}{m} V_\omega + \frac{1}{2m} (V_\sigma^2 - V_\omega^2), \quad (8)$$

where $V_{\sigma(\omega)}$ is the real part of the $\sigma(\omega)$ potential. Eqs. (7-8) show that in the standard mean-field approximation, when V_σ and V_ω do not depend on energy, the effective nucleon mass is also energy independent. The theoretical results of Ref. [6] can be phenomenologically reproduced by assuming that V_σ and V_ω are linear functions of E in an energy window of half-width, ΔE , of the order of 10 MeV centered at E_F . In addition, we shall make the same simplifying assumption as in Ref. [3], $dV_\sigma/dE = dV_\omega/dE = \alpha$, or, equivalently

$$V_{\sigma(\omega)} = V_{\sigma(\omega)}^0 + \alpha (E - E_F), \quad (|E - E_F| \leq \Delta E) \quad (9)$$

With this assumption, $m^*(E)$ becomes a linear function of E in the same energy window:

$$\frac{m^*(E)}{m} = 1 - 2\alpha - \frac{V_\omega^0}{m} (1 - \alpha) - \frac{V_\sigma^0}{m} \alpha + \frac{\alpha E_F}{m} - 2 \frac{\alpha E}{m}$$

$$|E - E_F| \leq \Delta E.$$

In the case of finite spherical nuclei, considered in Ref. [3] and in the present work, V_σ and V_ω are, of course, functions of the radial coordinate, and so are the Schrödinger equivalent potential, which contains additional r -derivative terms with respect to Eq. (8), and the effective nucleon mass. However, as opposed to the Dirac mass m_D , $m^*(r, E)$ might become greater than m , provided α is negative and large enough.

It is also important to point out that the present definition of m^* can be directly compared to the effective mass in non-relativistic models aimed at reproducing the empirical nuclear state densities, such as the model of Ref. [7] which accounts for the observed decrease of the level density parameter $a = \frac{\pi^2}{6} g(E_F)$ of the Bethe formula [1] with increasing excitation energy or temperature, from the average value of $A/8$ MeV $^{-1}$ at $T \leq 1$ MeV to $A/11$ MeV $^{-1}$ at $T \simeq 2.5$ MeV in the mass region $A \simeq 160$. Since the single-particle level density at the Fermi energy, $g(E_F)$, is empirically proportional to the mass number A and, in the model of Ref. [7], depends almost linearly on $m^*(E_F)$, we expect that our $m^*(E_F)$ is a smooth function of A in the same mass region. The density-averaged effective mass of Ref. [7] ranges from $1.12m$ at $A = 40$ to $1.13m$ at $A = 210$. These values are corroborated by a recent analysis [8] of neutron resonance spacings of several stable nuclei, which yields an average value $\langle m^*(E_F) \rangle /m = 1.09 \pm 0.13$.

If, according to Eq. (9), the effective potential in the Dirac equation (1) is a linear function of E , this defines a generalized eigenvalue problem

$$\hat{H}_D \psi = \bar{A} E \psi, \quad (10)$$

where \hat{H}_D is the energy independent Dirac Hamiltonian and \bar{A} denotes the matrix that contains the linear energy dependence. The problem can be solved exactly; the technical aspects of the solution are discussed in Ref. [3] and will not be repeated here.

We conclude this section by noting that, as is well known from non-relativistic theories, the energy dependence of the nucleon self-energy can be described microscopically in terms of the coupling of single-particle states to surface vibrations (see, e. g., Ref. [9]). This can be also done in a relativistic framework, by coupling the single-particle states generated in the energy-independent mean-field approximation to surface vibrations calculated in the relativistic random phase approximation. The present phenomenological approach can be considered as a preliminary quantitative evaluation of the impact of particle-vibration coupling on the calculation of total level densities in spherical nuclei.

3 Combinatorial Algorithm

Several techniques for an exact treatment of the problem of generating the full many-body physical state space for simple nuclear models can be found in the literature. An example is the odometer approach to the generation of multi-particle configurations adopted by Hillman and Grover [10], which is simple, but not efficient enough to be used in the case of heavy nuclei at high excitation energy. Recursive methods of calculating state and level densities of non-interacting many-fermion systems were proposed by various authors ([11], [12], [13]). Berger and Martinot [14] proposed the use of a five-variable generating function, whose power expansion coefficients determine the number of nuclear states with given numbers of proton particles, proton holes, neutron particles and neutron holes at a given excitation energy. This approach has been generalized by Hilaire, Delaroche and Girod [15] and applied to the calculation of nuclear level densities based on single-particle states that were generated by the density-dependent Gogny interaction in the self-consistent Hartree-Fock-Bogoliubov model. The approach of Ref. [15] and our work present some analogies, which will be discussed here and in the following sections.

The combinatorial method used in the present work is based on the Gaussian polynomial expansion of a generating function of states of n identical particles coupled to a given angular momentum, I . If the particles are either bosons of the same angular momentum, l , or fermions in the same j -shell, the problem of determining the multiplicities of states of given angular momentum projection, $I_z = M$, was solved long ago, and standard solutions can be found in textbooks (see, e. g., Ref.[16]).

The generating function appropriate to a system of fermions in the same j -shell is the following two-variable polynomial [17]:

$$F(q, t) = \prod_{i=1}^{2j+1} (1 + q^i t) = \sum_{r=0}^{2j+1} q^{r(r+1)/2} \begin{bmatrix} 2j+1 \\ r \end{bmatrix}_q t^r, \quad (11)$$

where the symbol in square brackets denotes the Gaussian polynomial in q of order $r(2j+1-r)$, which reduces to an ordinary binomial coefficient when $q = 1$. It can be proved that the multiplicity, $m(M)$, of states of n fermions with total angular momentum projection M is nothing but the coefficient of $q^{M+n(j+1)} t^n$ in formula (11), or, equivalently, the coefficient of q^M in

$$G(2j+1, n; q) = q^{-n(2j+1-n)/2} \begin{bmatrix} 2j+1 \\ n \end{bmatrix}_q. \quad (12)$$

Finally, the number of states of total angular momentum I is simply $N(I) = m(M=I) - m(M=I+1)$.

For the sake of completeness, we quote from Ref.[17] the generating function for states of bosons of angular momentum l :

$$B(q, t) = \prod_{i=1}^{2l+1} \frac{1}{1 - q^i t} = \sum_{r=0}^{\infty} q^r \begin{bmatrix} 2l+r \\ r \end{bmatrix}_q t^r. \quad (13)$$

In group-theoretical language, the above procedure corresponds to determining the multiplicities of $SU(2)$ representations occurring in the decomposition

$$SU(2j+1) \supset SU(2) \supset SO(2),$$

of the fully antisymmetric representation $\{1^n\}$ or the fully symmetric representation $\{n\}$ of $SU(2j+1)$ for fermions or bosons, respectively. The generating function approach is extended to the full Racah decomposition

$$SU(2j+1) \supset R(2j+1) \supset SU(2) \supset SO(2),$$

where $R(2j+1)$ is the seniority group (orthogonal for bosons and symplectic for fermions), on the basis of a simple consideration: if a state of an n -particle configuration of given angular momentum contains at least one zero-coupled pair, then the state appears also in the $(n-2)$ -particle configuration, because

the zero-coupled pair does not contribute to the angular momentum. As a consequence, the generating functions become [18]

$$V_b(2l + n, n; q) = G(2l + n, n; q) - G(2l + n - 2, n - 2; q), \quad (14)$$

and

$$V_f(2j + 1, n; q) = G(2j + 1, n; q) - G(2j + 1, n - 2; q), \quad (15)$$

for bosons and fermions, respectively, with $G(r, n; q)$ given by formula (12). and $n \leq (2j+1)/2$ in the fermion case, because of Pauli blocking. The generalization of the method to the multilevel case is straightforward: the generating function is the product of the generating functions (15) of individual levels.

This completes the formalism needed for the effective generation of the full state space that diagonalizes the schematic Hamiltonian

$$\hat{H} = \sum_i \hat{n}_i \epsilon_i + G \sum_i \hat{S}_+^{(i)} \hat{S}_-^{(i)}. \quad (16)$$

Here, \hat{n}_i denotes the number operator in the i -th single particle level with energy ϵ_i and angular momentum j_i . $\hat{S}_\pm^{(i)}$ are quasi-spin operators [19]. The model Hamiltonian consist of the usual mean-field part and a diagonal pairing interaction with constant strength G . The contribution of the pairing correlations to the total energy reads

$$E_P = -\frac{G}{4} \sum_i (n_i - s_i)(2j_i + 1 - n_i - s_i + 2). \quad (17)$$

It is important to note that our simplified residual pairing interaction conserves seniority, which is not realistic, but the implementation of the computational algorithm is straightforward. The present method represents an extension of the model with diagonal pairing in deformed doubly degenerate states, previously employed by Williams [20]. It has been shown [21] that the correlations in Eq. (17) can destabilize the shell model ground-state, inducing a transition to a superfluid phase.

In the Gaussian polynomial method (GPM) the calculation is scaled down from the number of states to the number of levels, and we emphasize that the method gives the exact state space for the model defined by Eq. (16), taking into account the full Racah decomposition of the many-body states with angular momentum projection M , seniority, energy, and parity as good quantum numbers.

The GPM is implemented in the computer program package SPINDIS [2], which contains various applications for calculating the total level (or state) densities and spin-parity distributions for the model defined by Eq. (16). By using recursion relations [17] for the coefficients in Eq. (15), SPINDIS allows high-speed computation. This part of the program, called distribution generator, is served by a many-body level-configuration generator consisting of four odometers, which control the following quantities:

- (1) pairs coupled to zero angular momentum, promoted among the available levels (with Pauli blocking taken into account);
- (2) unpaired particle configurations (input for the distribution generator);
- (3) number of unpaired protons (neutrons);
- (4) total number of broken pairs.

The energy corresponding to each many-body configuration is calculated by using the expression Eq. (17) for the pairing contribution. As it is well known, the basic problem in the generation of multi-particle configurations is that only a small fraction of the lexicographically generated levels is found below the chosen excitation energy cut-off. A detailed description of the algorithm for generating the multi-particle configurations is given in Ref. [2]. However, it is important to emphasize that the algorithm generates all possible states, i.e. not even a single state is lost up to the excitation energy cut-off. This is shown in Fig. 1, where we compare the total state density of ^{208}Pb up to 50 MeV calculated by the SPINDIS algorithm with the one calculated by the saddle-point approximation to the inverse Laplace transform of a grand-canonical fermion partition function. The latter approach to non-collective state density has been used for years, and is known to be very reliable, provided the excitation energy is not too low. Above the neutron binding energy, the numerical results are in very good agreement, so that the two methods are mutually corroborated. The input parameters of the calculation will be discussed in Section 5. We note that at the excitation energy of ≈ 50 MeV the state density $\omega \simeq e^{46} \text{ MeV}^{-1}$.

In addition to the total state density $\omega(E)$, SPINDIS computes the density of states of given spin projection $\omega(E, M)$, and the density of levels of given spin J

$$\rho(E, J) = \omega(E, M = J) - \omega(E, M = J + 1)$$

What is the maximum excitation energy at which calculations can be performed in our model? The single-nucleon wave functions are expanded in a spherical harmonic oscillator basis. This means that if too many oscillator shells were included in the calculation, the resulting nuclear state densities would steadily increase with energy. Nuclei have finite binding energies and state densities are expected to reach a maximum well below the dissociation region, and to decrease at higher excitation energies up to the dissociation point. Therefore, we can either truncate the sequence of single-particle levels

in such a way that yields a realistic behavior of total state densities when the excitation energy approaches the dissociation point, or we can limit our calculations to excitation energies that are well below the expected maximum, so that the resulting state densities are not very sensitive to the maximum number of single-particle orbitals included in the calculations.

In the present work we have chosen the simpler alternative. The calculations extend up to $E_{max} = 50$ MeV, which is of the order of magnitude of the nuclear potential well, and therefore of the maximum allowed one-hole energy. This excitation energy is much lower than $E^* \simeq 2A$ MeV, (A is the mass number) at which the physical state density already shows significant deviations from a simple Bethe formula like behavior. At even higher energies, the state density can be approximated by a Gaussian curve decreasing to 0 around $E^* \simeq 8A$ MeV [22]. An application of the state density formalisms to heavy ion reactions, where excitation energies between $2A$ and $8A$ MeV are easily attained, necessitates a physically sound prescription for the truncation of the single-particle level scheme. One possibility, suggested in Ref. [23], where use is made of the recursive algorithms of Ref. [13], is to include, in addition to bound states, only those neutron quasi-bound states that are below the centripetal barrier and the proton quasi-bound states that are below the Coulomb plus centripetal barrier or, alternatively, quasi-bound states that have optical-model transmission coefficients less than 0.05. A main default of the same work, however, is the use of a static mean field approximation, hardly justifiable at excitation energies above the pion production threshold, with the net result of overestimating the total state density at high excitation energy.

The extension of the present formalism to the energy region of interest in heavy ion reactions will be investigated in a future work.

4 Collective Enhancement

Until now we have explicitly considered only non-collective degrees of freedom in generating nuclear states at high excitation energy. The effective particle-vibration coupling that leads to realistic single-particle spectra around the Fermi energy is treated phenomenologically by an energy dependence of the effective single-nucleon potential and, therefore, of the effective nucleon mass.

It is well known, however, that collective nuclear excitations give a sizable contribution to the total state density at low excitation energy, and therefore must be included in the model space in order to have a meaningful comparison with experimental data. Since the present analysis is limited to spherical nuclei, the collective enhancement of the total state density will be mainly due to surface vibrations of various multipolarities. The lowest-lying vibrational modes are

the quadrupole, with spin-parity $L^\pi = 2^+$ and energy $E(2^+) \simeq 30A^{-2/3}$ MeV, and the octupole, with $L^\pi = 3^-$ and $E(3^-) \simeq 50A^{-2/3}$ MeV.

The effect of collective degrees of freedom on total state densities is conveniently illustrated by assuming the adiabatic decoupling of collective and non-collective excitations, approximately valid at excitation energies E much higher than the average, or characteristic, collective energy $\langle E_c \rangle$. This assumption is generally not valid in the energy range of interest to the present work, and is made here only for the sake of simplicity.

Let $\{E_c\}$ be the set of eigenvalues of a collective Hamiltonian. For any given eigenvalue E_c , the effective excitation energy available to non-collective modes, is $E^* = E - E_c$, and the total state density is obtained by summing the combinatorial state densities corresponding to all effective excitation energies

$$\begin{aligned} \omega_{tot}(E) &= \sum_c \omega(E - E_c) \\ &\simeq \sum_c \left[\omega(E) - E_c \frac{\partial \omega}{\partial E}(E) \right], \end{aligned} \quad (18)$$

provided that $E_c \ll E$. Let us introduce the temperature T corresponding to the excitation energy E , according to the definition

$$\frac{1}{T} = \frac{\partial}{\partial E} \ln \omega(E) = \frac{1}{\omega} \frac{\partial \omega}{\partial E}(E). \quad (19)$$

Eq. (18) can thus be rewritten in the form

$$\begin{aligned} \omega_{tot}(E) &\simeq \omega(E) \sum_c \left(1 - \frac{E_c}{T(E)} \right) \\ &\simeq \omega(E) \sum_c \exp \left(-\frac{E_c}{T(E)} \right) \\ &= \omega(E) Z_{coll}(E). \end{aligned}$$

The enhancement factor is the collective partition function $Z_{coll}(E)$ at temperature $T(E)$.

We emphasize that the above derivation is not based on the assumption that the fermion system is in equilibrium with an external heat and particle bath, as required by a grand-canonical ensemble description. On the contrary, our fermion system is isolated, since the non-collective state density ω is calculated by a combinatorial method consistent with a micro-canonical ensemble description, and the definition (19) of temperature is based on Boltzmann's

definition of entropy, $S(E) = \ln \omega(E) + c$, valid in the micro-canonical ensemble.

As was pointed out in Ref. [24], the above micro-canonical description can be transformed into a grand-canonical one by observing that $S(E) = S_{gc}(E) + \Delta S(E)$, where $\Delta S(E)$ goes to zero for $E \rightarrow \infty$. Thus,

$$\frac{1}{T_{gc}} \equiv \frac{\partial S_{gc}}{\partial E}(E) = \frac{1}{T} - \frac{\partial \Delta S}{\partial E}(E) > \frac{1}{T}. \quad (20)$$

As a consequence we expect that, as soon as the excitation energy is high enough for a grand-canonical description to become applicable, the fermion system can be considered in thermal equilibrium with an external reservoir at a temperature $T_{gc}(E)$, systematically lower than the micro-canonical temperature T , derived from the combinatorial state density ω , at the same energy E . This is confirmed by Fig. 2, which compares the grand-canonical and micro-canonical temperatures of ^{208}Pb as functions of E . We note that the micro-canonical temperature has been obtained by numerical derivation of an energy-smoothed state density, in order to avoid numerical divergence at energies where the original combinatorial state density displays discontinuities connected with the opening of particle-hole excitation channels. More precisely, formula (19) predicts divergence of inverse temperature, and, consequently, a sudden temperature dip at any discontinuity connected with a new particle-hole excitation, followed by a zero inverse temperature, and then a diverging temperature, in the plateau between two successive discontinuities of the state density. The rapid oscillations of the micro-canonical temperature derived from a state density computed in energy bins, ΔE , as small as 500 KeV, are progressively washed out with increasing ΔE up to 2 MeV, where good agreement is reached with the grand-canonical temperature corresponding to the same excitation energy.

A non monotonic behaviour of temperature as a function of excitation energy was experimentally observed for the first time in the level densities of well deformed lanthanides below 6 MeV [25] and, more recently, also in the level densities of weakly deformed Sm isotopes [26] and attributed to progressive breaking of nucleon pairs, and, at higher energies, quenching of pair correlations. Although this effect has not been observed till now in magic nuclei, where the discontinuities in level densities should be connected with non-collective particle-hole excitations across shell closures, a proper extension of the micro-canonical formalism to open-shell nuclei would make it possible to compare calculated temperature fluctuations with those extracted from experimental data, thus giving an important advantage at low excitation energies over a canonical formalism, where temperature fluctuations are smoothed out by construction.

If the derivative in Eq. (20) is approximated by

$$\frac{\partial \Delta S}{\partial E} \simeq \frac{\delta S}{\delta E}, \quad (21)$$

the expression can be rewritten as

$$\frac{\delta E}{T} \simeq \frac{\delta E}{T_{gc}} - \delta S, \quad (22)$$

i.e. it relates a change in excitation energy in the micro-canonical system with a change of energy and entropy in the grand-canonical frame.

Once we are allowed to reformulate the equilibrium of our fermion system in a grand-canonical language, it becomes natural to express the collective enhancement factor, Z_{coll} , in terms of a boson system in equilibrium with fermions at temperature $T_{gc}(E)$. The bosons represent collective fermion pairs treated in the random phase approximation (RPA), as shown in Ref. [27], where the vibrational factor is expressed in terms of the energy and entropy of a gas of RPA phonons of both parities π_i , and all multipolarities λ_i

$$Z_{coll}(T_{gc}(E)) = \exp \left(\delta S - \frac{\delta E}{T_{gc}} \right), \quad (23)$$

where

$$\begin{aligned} \delta E &= \sum_i \sum_{\pi_i} (2\lambda_i^{(\pi_i)} + 1) n_i \omega_i, \\ \delta S &= \sum_i \sum_{\pi_i} (2\lambda_i^{(\pi_i)} + 1) [(1 + n_i) \ln(1 + n_i) - n_i \ln n_i]. \end{aligned}$$

ω_i is the energy of the RPA phonon of type i , with spin-parity $\lambda_i^{(\pi_i)}$. In the present analysis we only consider the leading modes of both parities, namely the quadrupole ($\lambda_i^{(\pi_i)} = 2^+$) and the octupole ($\lambda_i^{(\pi_i)} = 3^-$). The average number of type- i phonons is given by a Bose distribution corrected for damping effects [28]:

$$n_i(T) = \frac{\exp \left[-\frac{\gamma_i(T)}{2\omega_i} \right]}{\exp \left(\frac{\omega_i}{T} \right) - 1}, \quad (24)$$

where the temperature dependence of the damping factor γ_i is taken from the Landau theory of Fermi liquids. The numerical coefficients are determined by

a consistent description of collective levels and neutron resonance data [29]

$$\gamma_i(T) \simeq 0.0075 A^{\frac{1}{3}} \left[(\omega_i)^2 + 4\pi^2 T^2 \right] \quad \text{MeV} \quad (25)$$

In the limit $T \rightarrow \infty$, Eqs. (24) and (25) give $n_i \rightarrow 0$ and, consequently $\lim_{T \rightarrow \infty} Z_{coll} = 1$.

In principle, because the combinatorial algorithm [17] exploited by SPINDIS can be also applied to bosons, as illustrated in the previous section, the vibrational enhancement can be described directly in the micro-canonical frame. A similar procedure is followed in Ref. [15], where a three-variable generating function is used, whose expansion coefficients give the multiplicities of states of given boson number and spin projection at a given excitation energy. In the latter approach, however, the damping of collectivity, which is quite natural in the finite temperature description of Eq. (24), is introduced by truncating *ad hoc* the boson generating function at $n_{max} = 3$, with the justification that states with higher boson number are rather weakly collective.

Neither of the two approaches to the vibrational enhancement is, however, very satisfactory from a theoretical point of view. Both treat the excited nucleus as an assembly of independent fermions and bosons. This approximation might be acceptable, and is confirmed *a posteriori* by comparison with experimental data, if we limit ourselves to the calculation of total level densities. A reliable description of partial level densities of given spin and parity, on the other hand, necessitates a consistent treatment of the boson-fermion interaction, by taking properly into account the microscopic structure of bosons as collective fermion pairs.

The present analysis is limited only to spherical nuclei, and, consequently, only the vibrational enhancement of state densities is taken into account, because our main goal is to check the validity of the relativistic mean-field approach to excited systems where correlation effects, not yet easily treatable in a relativistic framework, play a minor role. As is known, the extension to deformed nuclei will require, in addition, a rotational enhancement, as well as an appropriate treatment of the coupling of rotations and vibrations. The latter coupling is frequently neglected in level density calculations, thus leading to a significant overestimate of the collective enhancement around its maximum, as shown in a recent evaluation [30] of this effect in the framework of the interacting boson model.

A fully grand-canonical description of both single-particle and collective degrees of freedom in nuclear level densities smooths out the low energy fluctuations connected with the onset of non-collective particle-hole excitations and approaches the micro-canonical description with increasing excitation energy.

A self-consistent mean-field approach to nuclear level densities in the grand-canonical framework is presented in Ref. [31]. There, the single-nucleon states are calculated in the Skyrme-Hartree-Fock approximation by means of the MSk7 effective interaction and the pairing interaction is treated in the standard BCS approximation. The average effective mass turns out to be $\langle m^* \rangle \simeq 1.05m$. A temperature-dependent rotational enhancement of standard form is taken into account in the level densities of strongly deformed nuclei. Although the calculation does not include any explicit vibrational enhancement for spherical nuclei, this effect is implicitly taken into account by adjusting excitation energy and entropy so as to reproduce empirical data, such as the cumulative numbers of discrete levels and the neutron resonance spacings. This study, however, is neither limited to the about 300 nuclei whose neutron resonance spacings are measured, nor to the about 1200 nuclei whose discrete spectra are known to some extent, but, aiming at astrophysical applications, is extended to 8000 nuclei outside the beta-stability valley, where extrapolation of empirical systematics would not make any sense. Total and spin-dependent level densities are provided in tabular form up to an excitation energy of 150 MeV.

A new promising approach to nuclear level densities in the canonical framework is provided by the shell-model Monte Carlo (SMMC) method [32]. There, use is made of the Hubbard-Stratonovich representation for the $e^{-\beta H}$ operator, β being the inverse temperature, and the energy of the system, E , is computed by the auxiliary field method as a function of β from the canonical expectation value of the Hamiltonian through an exact particle-number projection of both protons and neutrons. The partition function, $Z(\beta)$, is then determined by numerical integration of $E(\beta)$ and the level density obtained as the inverse Laplace transform of Z , in the saddle-point approximation. Using in their Hamiltonian a separable surface-peaked residual interaction, in addition to the standard pairing interaction, active in the $(pf+0g_{9/2})$ valence shell, the authors of Ref. [32] were able to reproduce the experimental level density of ^{56}Fe up to 20 MeV, thus treating collective and non-collective excitations on the same computational basis, without resorting to any external enhancement factor. The parity-projected level densities in the above mentioned range were well reproduced by back-shifted Bethe formulae with parity-dependent parameters.

The SMMC method was later applied to other even-even nuclei, from Fe to Ge [33], as well as to odd-mass and odd-odd nuclei [34] in the same mass region and energy range. In the case of odd fermion systems, the weight functions appearing in the auxiliary field integrals are not necessarily positive, thus giving rise to a well-known sign problem, recently overcome by the particle-number reprojection method [35]. All the above mentioned SMMC calculations are well reproduced by back-shifted Bethe formulae, which are thus able to fit theoretical level densities which include correlations among nucleons, at least

for nuclei which are not strongly deformed, in an energy range of the order of some ten MeV.

The possibility to include correlations in the Bethe formula has been known empirically for years, and is reflected in the fact, already quoted in Section 2, that the average value of the level density parameter at the neutron binding energy, $a = A/8 \text{ MeV}^{-1}$, is about as twice as the value predicted by the Fermi gas model, thus accounting for low energy correlations other than those described by the energy backshift. A theoretical justification of the validity of the shifted Bethe formula beyond the independent particle approximation was recently given in Ref. [36]. There, it was shown that the shifted Bethe formula is closely connected with a continuous binomial level density in a finite space, defined by three parameters, which can be extracted from the three lowest moments of a Hamiltonian of any rank.

We believe, however, that the mean-field approach to nuclear level densities is still worthy of development and applications, were it not for the fact that the SMMC method is still very far from applicability to a region of the periodic chart and to an energy range as large as those allowed in a self-consistent mean-field approximation (see, in particular, Ref. [31]). Moreover, at excitation energies higher than about 2 MeV/nucleon, easily attainable in current heavy ion reactions, we expect not only vanishing correlations, but also failure of the Bethe formula, which predicts an exponentially increasing level density, physically unreasonable at excitation energies approaching the nuclear binding energy, as already discussed at the end of the previous section. Under such extreme conditions, microcanonical, or canonical calculations based on a self-consistent relativistic mean-field approximation may prove a very valuable approach, as we intend to show in a future work.

5 Numerical Results

In this section we discuss and compare with experimental data the results of illustrative calculations of total level densities of few magic and semi-magic nuclei.

A crucial parameter of our calculations is the density of single-particle states at the Fermi energy. The single-nucleon spectra are calculated with the relativistic mean-field model with energy-dependent effective mass. For the initial parameterization of the effective Lagrangian (meson masses and meson-nucleon couplings) we have chosen, instead of the NL3 effective interaction [37] adopted in Ref. [3], the older parameter set NL1 [38]. Even though NL1 is admittedly inferior to NL3 in reproducing the bulk nuclear properties, it yields a more realistic magic gap $E(h_{9/2}) - E(s_{1/2})$ in ^{208}Pb , considered also in

the present work. For this reason, NL1 has also been adopted as the starting parameterization in the recent analysis [39] of shape coexistence phenomena in the Pt-Hg-Pb region.

In addition, the half-width of the interval in which the σ and ω mean-field potentials are assumed to be linearly dependent on energy, has been reduced from 10 to 5 MeV. In this way, we obtain more realistic energies of the single-particle states above the Fermi surface, which have a particularly strong effect on the calculated total level densities.

The linear energy dependence of the σ and ω mean-field potentials is determined by the parameter α in Eq. (9).

The input parameters used in the calculation of three illustrative cases, ^{208}Pb , ^{114}Sn and ^{60}Ni , are collected in Table 1 (parameters of the relativistic mean-model), and Table 2 (the parameters α of the energy-dependent effective mass, the pairing strengths and the phonon energies).

Starting from the heaviest nucleus, ^{208}Pb , α has been adjusted so as to reproduce the binding energy, the cumulative number of discrete levels as a function of excitation energy, and the s -wave neutron resonance spacing, D_{obs} , measured in the $^{207}\text{Pb} + n$ reaction. As is known, in the case of an odd-mass target nucleus with N neutrons and ground-state spin-parity I^π ,

$$D_{obs} = \frac{1}{\rho(B_n, J = I + 1/2, \pi) + \rho(B_n, J = I - 1/2, \pi)}, \quad (26)$$

where B_n and $\rho(U, J, \pi)$ are, respectively, the neutron binding energy and the density of levels with spin-parity J^π of the compound nucleus with $N + 1$ neutrons. Since no experimental data are available on the total level density at higher excitation energy, we have checked the quality of our calculations by comparing the total state density obtained from the SPINDIS algorithm applied to the set of experimental single-particle levels, already adopted in Ref. [3], with the analogous level density obtained with the same algorithm applied to the single-particle levels generated in the RMF approximation with non-zero α parameter. The agreement is excellent over the whole energy range considered in the present work.

The theoretical non-collective level density thus obtained has been multiplied by the vibrational enhancement factor described in the previous section, by assuming quadrupole and octupole phonon energies close to the energies of the 2_1^+ and 3_1^- levels, respectively, somewhat different, for a bi-magic nucleus, from the values expected from systematics.

The resulting total state density is compared in Fig. 3 with the corresponding grand-canonical calculation of Ref. [31]. The agreement appears to be satisfac-

tory up to about 20 MeV, while our level density becomes larger than that of Ref. [31] with increasing excitation energy. It is worthwhile to stress, however, that Ref. [31] does not include an explicit vibrational enhancement factor for spherical nuclei. Experimental and calculated cumulative numbers of discrete levels at low excitation energy are compared in the inset of the same figure.

In order to check the possibility of reproducing our numerical results with simple analytic formulae, we have compared the energy trend of our total state density with the standard backshifted Bethe formula (BBF) [46]:

$$\omega_T^{\text{BBF}}(E) = g \frac{\sqrt{\pi}}{24} \frac{\exp \left[2\sqrt{a(E - E_0)} \right]}{a^{1/4}(E - E_0)^{5/4}}, \quad (27)$$

and with the generalized Bethe formula (GBF) [47]:

$$\omega_T^{\text{GBF}}(E) = g \frac{\sqrt{\pi(1 - \xi)}}{6\sqrt{8}} \cdot \frac{\exp \{ [a(E - E_0)]^\xi / \xi \}}{(E - E_0)[a(E - E_0)]^{1-3\xi/2}}. \quad (28)$$

In both formulae, the total state density is obtained for $g = 2$. Moreover, GBF reduces to BBF for $\xi = 0.5$.

The BBF and GBF fits to the numerical state density of ^{208}Pb are shown in Fig. 4 and the corresponding parameters, adjusted on the energy range from 10 to 30 MeV, are given in Table 3. Our numerical results are well reproduced by GBF on the whole energy range up to 50 MeV, while BBF exhibits sizable discrepancies outside the region of fit. The BBF curve appears to be in better agreement with the total state density of Ref. [31], probably in connection with the fact that the latter does not include an explicit vibrational enhancement.

For lighter spherical nuclei, there are experimental data on total level densities mainly below 20 MeV, where the vibrational enhancement factor discussed in Section 4 is expected to play a significant role. This is indeed the case for the semi-magic nuclei ^{114}Sn and ^{60}Ni , whose calculated level densities are compared with experimental data in Figs. 5 and 6, respectively. Here, α is adjusted again on the binding energy and the cumulative number of discrete levels, while the level density at higher energy is reproduced by means of the smooth vibrational factor discussed in the previous section.

The total state densities including collective effects are equally well reproduced by BBF and GBF with the parameters given in Table 3 up to about 40 MeV, while the damping of the collective factor with increasing energy yields systematically lower results than BBF and GBF at higher excitation. These results are in qualitative agreement with the conclusions of Ref. [36] about the range of validity of BBF.

The relativistic mean-field model, the combinatorial algorithm and the vibrational enhancement factor adopted in the present work are strictly valid for spherical nuclei only. In order to investigate the possible extension to open shell nuclei, we have performed calculations also for slightly deformed nuclei in the $A = 60$ mass region, in particular ^{56}Fe and ^{55}Mn , for which experimental data of the same quality as ^{60}Ni are available.

Comparison of calculated and experimental level densities, shown in Figs. 7 and 8 for ^{56}Fe and ^{55}Mn , respectively, indicates, however, that for open-shell nuclei there are some problems still to be solved. To bring these problems into focus, level densities have been calculated with $\alpha = 0$ and are plotted without any collective enhancement factor.

In general, total level densities below 10 MeV turn out to be slightly overestimated by our calculation, as a consequence of the degeneracy of the ground state, as shown by the insets of Figs. 7 and 8, where calculated and experimental cumulative number of levels are compared. The low energy data are derived from the cumulative number of discrete levels, whose spectra are somewhat different from those of spherical nuclei. In particular, both ^{56}Fe and the even-even core of ^{55}Mn , i. e. ^{54}Cr , show a ground-state rotational band including the 2_1^+ , 4_1^+ , 6_1^+ and 8_1^+ states, while the energy of the 2_2^+ state is of the order of magnitude of the quadrupole phonon energy from phenomenological systematics.

It is not expected that the single-particle level scheme from a mean field with spherical symmetry and the combinatorial SPINDIS algorithm for spherical nuclei adopted in the present work produce a very realistic distribution of non-collective states at low energy, neither can a simple vibrational enhancement factor compare well with the experimental level densities above 15 MeV, where both vibrational and rotational degrees of freedom are simultaneously excited and coupled together.

Therefore, necessary conditions for extension of the present mean-field approach to open-shell nuclei appear to be the evaluation of single-particle level schemes at realistic deformations and the use of a combinatorial algorithm, such as the recursive one [11,13], valid also for deformed systems. Once a more realistic single-particle scheme is obtained, more reliable conclusions can be drawn about the treatment of the particle-vibration coupling, simulated by the α parameter of our model. Corresponding calculations [48] of the effective nucleon mass in a cranked Nilsson-BCS approach to the structure of statically deformed nuclei show that the frequency dependent factor, the so-called ω mass, m_ω , of the effective nucleon mass is somewhat different from that obtained for open-shell nuclei with spherical symmetry, i. e. the one that could be simulated with the present version of our model.

Moreover, the derivation of a collective enhancement factor for deformed nuclei is nontrivial and requires an investigation of the effect of coupling of different collective modes, such as rotations and surface vibrations, not only with the fermion degrees of freedom, but also among themselves. The latter coupling, often neglected in the level density formalisms, is expected to play an important role in the energy range considered in the present work.

For the sake of comparison, we show in Figs. 7 and 8 also the level density resulting from the NL3 parametrization given in Tab. 1. NL1 turns out to be in slightly better overall agreement with the experimental data.

6 Conclusions and Perspectives

The relativistic mean-field model with energy-dependent effective mass, introduced in Ref. [3], exhibits realistic densities of single-nucleon states at the Fermi energy. When coupled to the combinatorial algorithm SPINDIS for treating non-collective excitations of a spherical nucleus, and to a simple vibrational partition function for collective excitations, the model yields total level densities in agreement with experimental data in magic and semi-magic nuclei.

In the present form, however, the model contains a phenomenological treatment of surface vibrations and of their coupling to the single-particle degrees of freedom. A fully microscopic formulation would require generation of phonons in a relativistic RPA approximation and explicit formulation of the particle-vibration coupling, presently simulated by the linear energy dependence of the meson fields.

The planned extension to non-magic deformed nuclei, necessary for the present approach to become competitive with the non-relativistic mean-field approaches [15,31], requires calculation of deformed single-particle schemes, an appropriate combinatorial algorithm and a collective factor taking into account rotational and vibrational degrees of freedom, and their coupling as a function of excitation energy, or temperature.

There is, moreover, a kind of level density problem where the relativistic mean-field approach should have no true competitors, i. e. the calculation of nuclear level densities above the threshold of pion production and up to the total binding energy of the system, where a static non-relativistic mean-field approximation loses its validity. The present linear energy dependence of the classical meson fields is, admittedly, a low-energy approximation, to be properly modified on the basis of the results of the relativistic Brückner-Hartree-Fock theory [6], which predicts a faster decrease of the real potential well

with increasing excitation energy and, consequently, a sizable change of the single-particle level scheme, as well as the formation of an imaginary potential well, whose depth is expected, on the basis of the Dirac phenomenology analysis of the scattering of polarized intermediate-energy nucleons , to increase quadratically with energy above the threshold of pion production.

An important step in this direction is provided by Ref. [49], where a relativistic optical potential suited to proton-nucleus scattering at intermediate energies is derived in the frame of a relativistic mean field model with density-dependent meson-nucleon couplings. The rearrangement contributions to the nucleon self-energies, due to the density dependence of the meson-nucleon couplings, are necessary in order to get a thermodynamically consistent theory. These effects could be introduced in the present model along the lines of Ref. [50], where a new density-dependent parametrization, DD-ME1, has been applied with success to the description of various properties of magic and semi-magic nuclei, and could lend itself to an extension to open-shell nuclei without conceptual difficulties.

References

- [1] H. A. Bethe, Rev. Mod. Phys. 9 (1937) 69.
- [2] D. K. Sunko, Comput. Phys. Comm. 101 (1997) 171.
- [3] D. Vretenar, T. Nikšić, and P. Ring, Phys. Rev. C 65 (2002) 024321.
- [4] B. D. Serot and J. D. Walecka, Adv. Nucl. Phys. 16 (1986) 1.
- [5] M. Jaminon and C. Mahaux, Phys. Rev. C 40 (1989) 354.
- [6] M. Jaminon and C. Mahaux, Phys. Rev. C 41 (1990) 697.
- [7] S. Shlomo and J. B. Natowitz, Phys. Rev. C 44 (1991) 2878.
- [8] S. F. Mughabghab and C. Dunford, Phys. Rev. Lett. 81 (1998) 4083.
- [9] A. Bohr and B. R. Mottelson, Nuclear Structure, Vol. II, Benjamin, Reading, MA, New York, 1975.
- [10] M. Hillman, J. R. Grover, Phys. Rev. 185 (1969) 1303.
- [11] F. C. Williams, Nucl. Phys. A 133 (1969) 33.
- [12] K. Albrecht and M. Blann, Phys. Rev. C 8 (1973) 1481.
- [13] C. Jacquemin and S. K. Kataria, Z. Phys. A 324 (1986) 261.
- [14] J. F. Berger and M. Martinot, Nucl. Phys. A 226 (1974) 391.
- [15] S. Hilaire, J. P. Delaroche, and M. Girod, Eur. Phys. J. A 12 (2001) 169.

- [16] A. De-Shalit and I. Talmi, Nuclear Shell Theory, Academic Press, New York, 1963.
- [17] D. K. Sunko and D. Svrtan, Phys. Rev. C 31 (1985) 1929.
- [18] D. K. Sunko, Phys. Rev. C 35 (1987) 1936.
- [19] P. Ring and P. Schuck, The Nuclear Many Body Problem, Springer, New York, 1980.
- [20] F. C. Williams, Nucl. Phys. A 166 (1971) 231.
- [21] D. K. Sunko, Ann. Phys. 199 (1990) 227.
- [22] S. M. Grimes, Phys. Rev. C 42 (1990) 2744.
- [23] M. G. Mustafa, M. Blann, A. V. Ignatyuk, and S. M. Grimes, Phys. Rev. C 45 (1992) 1078.
- [24] D. J. Morrissey, W. Benenson, and W. A. Friedman, Annu. Rev. Nucl. Part. Sci. 44 (1994) 27.
- [25] E. Melby, L. Bergholt, M. Guttormsen, M. Hjorth-Jensen, F. Ingebretsen, S. Messelt, J. Rekstad, A. Schiller, S. Siem, and S. W. Ødegård, Phys. Rev. Lett. 83 (1999) 3150.
- [26] S. Siem, M. Guttormsen, K. Ingeberg, E. Melby, J. Rekstad, A. Schiller, and A. Voinov, Phys. Rev. C 65 (2002) 044318.
- [27] A. V. Ignatyuk, Yad. Fiz. 21 (1975) 20.
- [28] V. P. Lunev, Yu. N. Shubin, C. Grandi, B. Poli, and A. Ventura, Nuovo Cimento A112 (1999) 743.
- [29] A. I. Blokhin, A. V. Ignatyuk, and Yu. N. Shubin, Yad. Fiz. 48 (1988) 371.
- [30] A. Mengoni, A. Ventura, S. Masetti, R. Capote, and D. Kusnezov, J. Nucl. Sci. Technol. Suppl. 2 (2002) 766.
- [31] P. Demetriou and S. Goriely, Nucl. Phys. A 695 (2001) 95.
- [32] H. Nakada and Y. Alhassid, Phys. Rev. Lett. 79 (1997) 2939.
- [33] H. Nakada and Y. Alhassid, Phys. Lett. B 436 (1998) 231.
- [34] K. Langanke, Phys. Lett. B 438 (1998) 235.
- [35] Y. Alhassid, S. Liu, and H. Nakada, Phys. Rev. Lett. 21 (1999) 4265.
- [36] A. P. Zuker, Phys. Rev. C 64 (2001) 021303.
- [37] G. A. Lalazissis, J. König, and P. Ring, Phys. Rev. C 55 (1997) 540.
- [38] P. G. Reinhard, M. Rufa, J. Maruhn, W. Greiner, and J. Friedrich, Z. Phys. A 323 (1986) 13.

- [39] T. Nikšić, D. Vretenar, P. Ring, and G. A. Lalazissis, Phys. Rev. C 65 (2002) 054320.
- [40] F. Tondeur, Nucl. Phys. A 315 (1979) 353.
- [41] N. Cerf, Phys. Rev. C 50 (1994) 836.
- [42] A. Mengoni and Y. Nakajima, J. Nucl. Sci. Technol. 31 (1994) 61.
- [43] C. L. Dunford, T. W. Burrows, Online nuclear data service, <http://www.nndc.bnl.gov/nndc/nudat/>.
- [44] D. R. Chakrabarty, V. M. Datar, S. Kumar, E. T. Mirgule, H. H. Oza, and U. K. Pal, Phys. Rev. C 51 (1995) 2942.
- [45] A. S. Iljinov, M. V. Mebel, N. Bianchi, E. D. Santcis, C. G. V. Lucherini, V. Muccifora, E. Polli, A. R. Reolon, and P. Rossi, Nucl. Phys. A 543 (1992) 517.
- [46] T. Von Egidy, H. H. Schmidt, and A. N. Behkami, Nucl. Phys. A 454 (1986) 109.
- [47] V. Paar and R. Pezer, Phys. Lett. B 411 (1997) 19.
- [48] P. Donati, T. Døssing, Y. R. Shimizu, S. Mizutori, P. F. Bortignon, R. A. Broglia, Phys. Rev. Lett. 84 (2000) 4317.
- [49] S. Typel, O. Riedl and H. H. Wolter, Nucl. Phys. A 709 (2002) 299.
- [50] T. Nikšić, D. Vretenar, P. Finelli and P. Ring, Phys. Rev. C 66 (2002) 024306.
- [51] C. C. Lu, L. C. Vaz, and J. R. Huizenga, Nucl. Phys. A 190 (1972) 229.

Table 1

The parameter sets of the relativistic mean-field model.

Parameter	NL1	NL3
m_n/MeV	938.000	939.0000
m_σ/MeV	492.250	508.1941
m_ω/MeV	795.359	782.5010
m_ρ/MeV	763.000	763.0000
g_σ	10.138	10.2169
g_2/fm^{-1}	-12.172	-10.4307
g_3	-36.265	-28.8851
g_ω	13.285	12.8675
g_ρ	4.975	4.4744

Table 2

Parameters of the linear energy dependence of the effective nucleon mass, pairing strengths (from Refs. [40,41]), and phonon energies ($E(2^+) = 30/A^{2/3}$ MeV, $E(3^-) = 50/A^{2/3}$ MeV) used in this work. For ^{208}Pb the quadrupole and octupole phonon energies are the experimental energies of the 2_1^+ and 3_1^+ levels, respectively. The latter is the first excited level, and systematics do not give the correct order of levels.

Nuclei	$\alpha(\text{SE})$	G_n [MeV]	G_p [MeV]	$E(2^+)$ [MeV]	$E(3^-)$ [MeV]
^{208}Pb	-0.2	0.076	0.091	4.085	2.615
^{114}Sn	-0.3	0.12	0.13	1.276	2.127
^{60}Ni	-0.1	0.21	0.19	1.957	3.262

Table 3

Fits of the BBF (27) and GBF (28) parameters to the calculated total state densities.

Nuclei	BBF			GBF			
	a [MeV $^{-1}$]	E_0 [MeV]	χ^2	a [MeV $^{-1}$]	E_0 [MeV]	ξ	χ^2
^{208}Pb	13.000	6.000	0.14	4.717	2.466	0.6354	0.015
^{114}Sn	12.16	-0.384	0.044	28.064	2.643	0.4226	0.01
^{60}Ni	6.346	-0.228	0.08	4.634	-1.719	0.5410	0.08

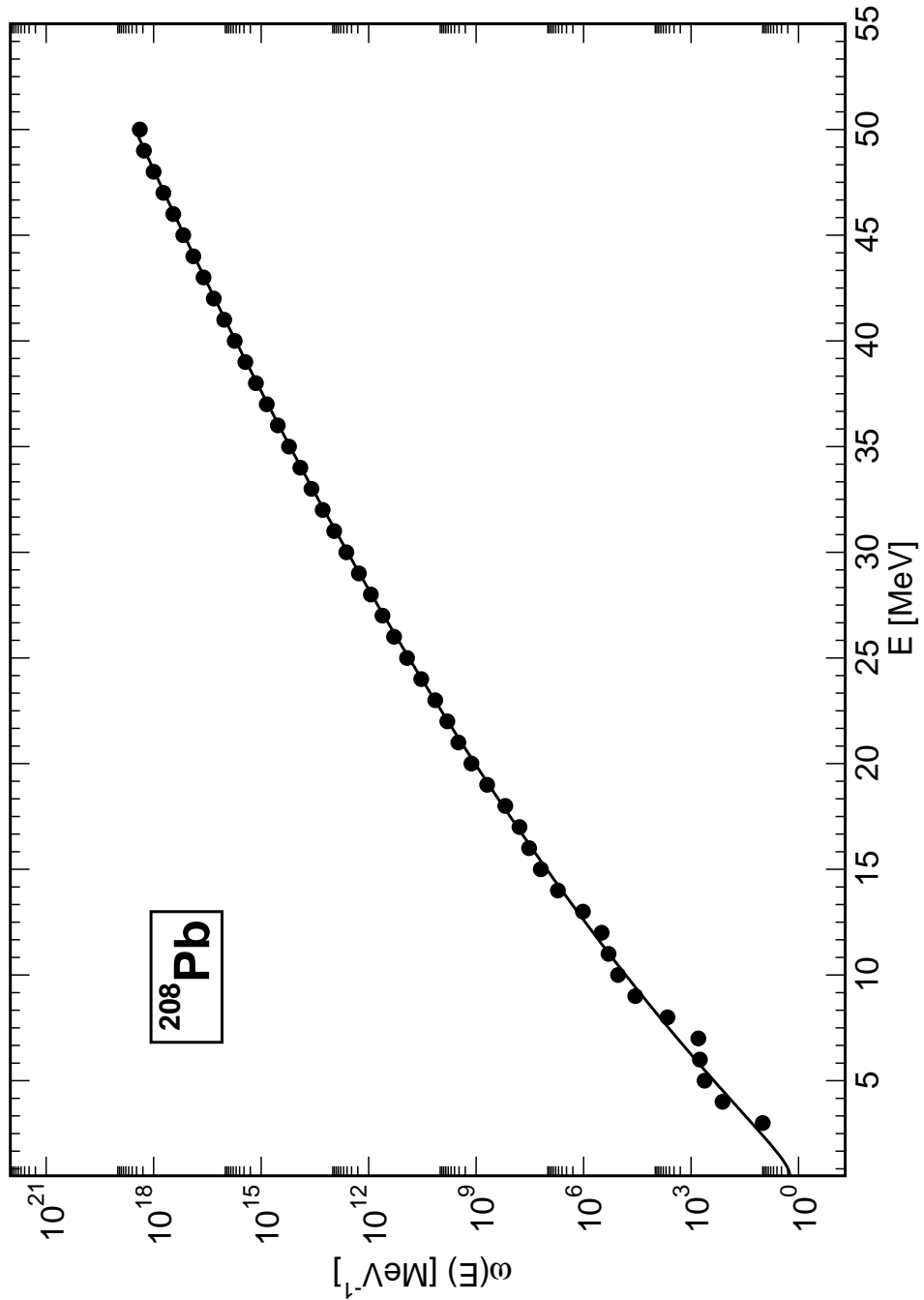


Fig. 1. Comparison of the total state density of ^{208}Pb computed with the SPINDIS algorithm (dots), and with the saddle-point method (solid line), using a set of realistic single particle levels calculated with the relativistic mean-field model with energy dependent effective mass.

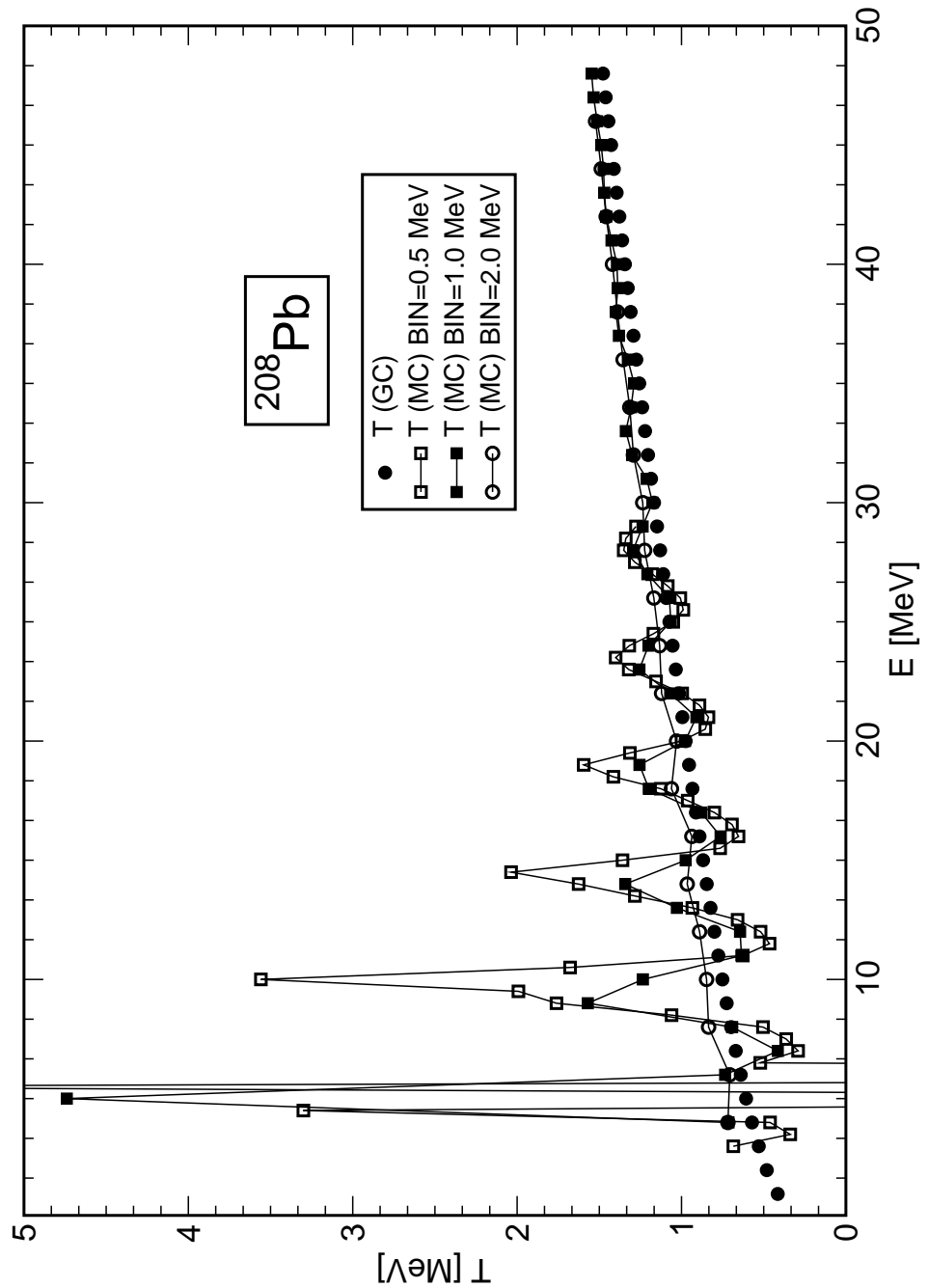


Fig. 2. Comparison of the energy averaged micro-canonical temperature T (for three different values of the energy bin), and the grand-canonical temperature T_{gc} , as functions of E for ^{208}Pb .

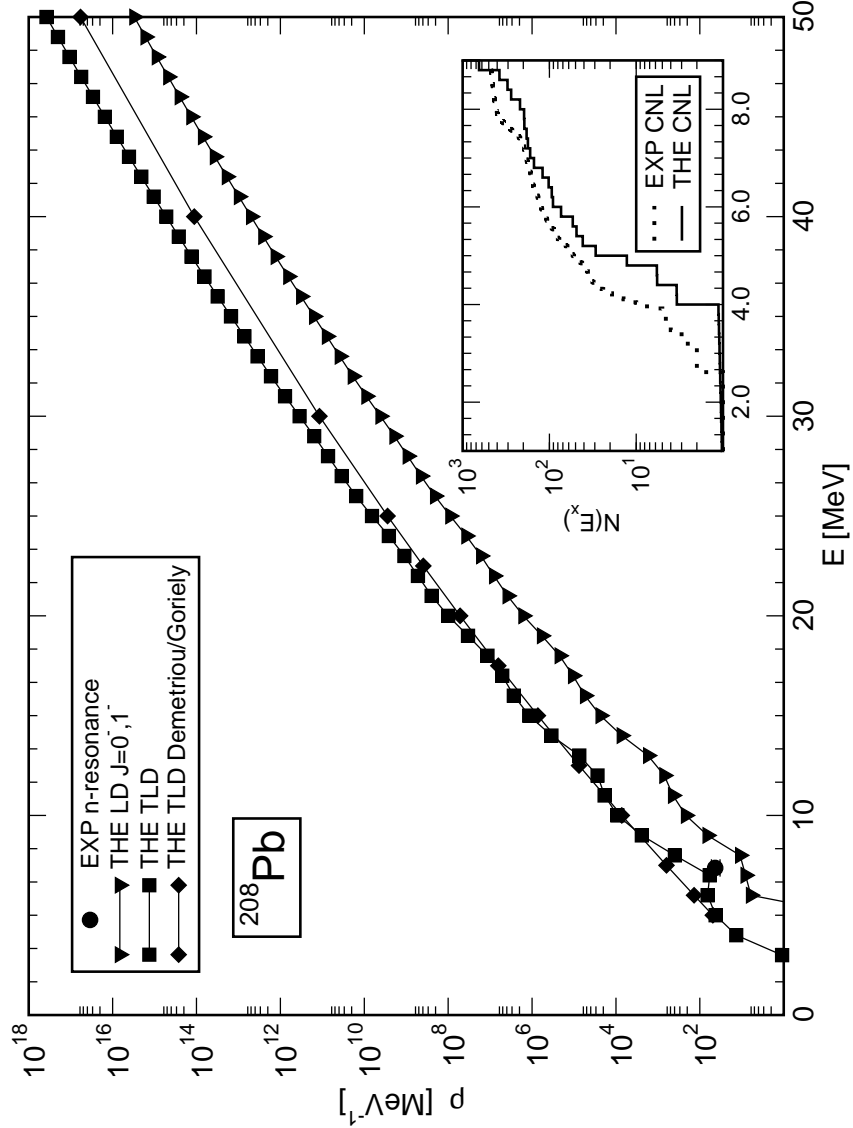


Fig. 3. Level densities of ^{208}Pb as functions of the excitation energy: a) total level density (TLD) (squares); b) sum of the partial level densities for $J^\pi = 0^-$ and $J^\pi = 1^-$ (triangles), compared with the experimental s -wave neutron resonance density of the $^{207}\text{Pb} + n$ reaction (circle) [42]; c) total level density from Ref. [31] (diamonds). In the inset the calculated cumulative numbers of discrete levels (CNL) (solid line) are shown in comparison with the experimental values [43].

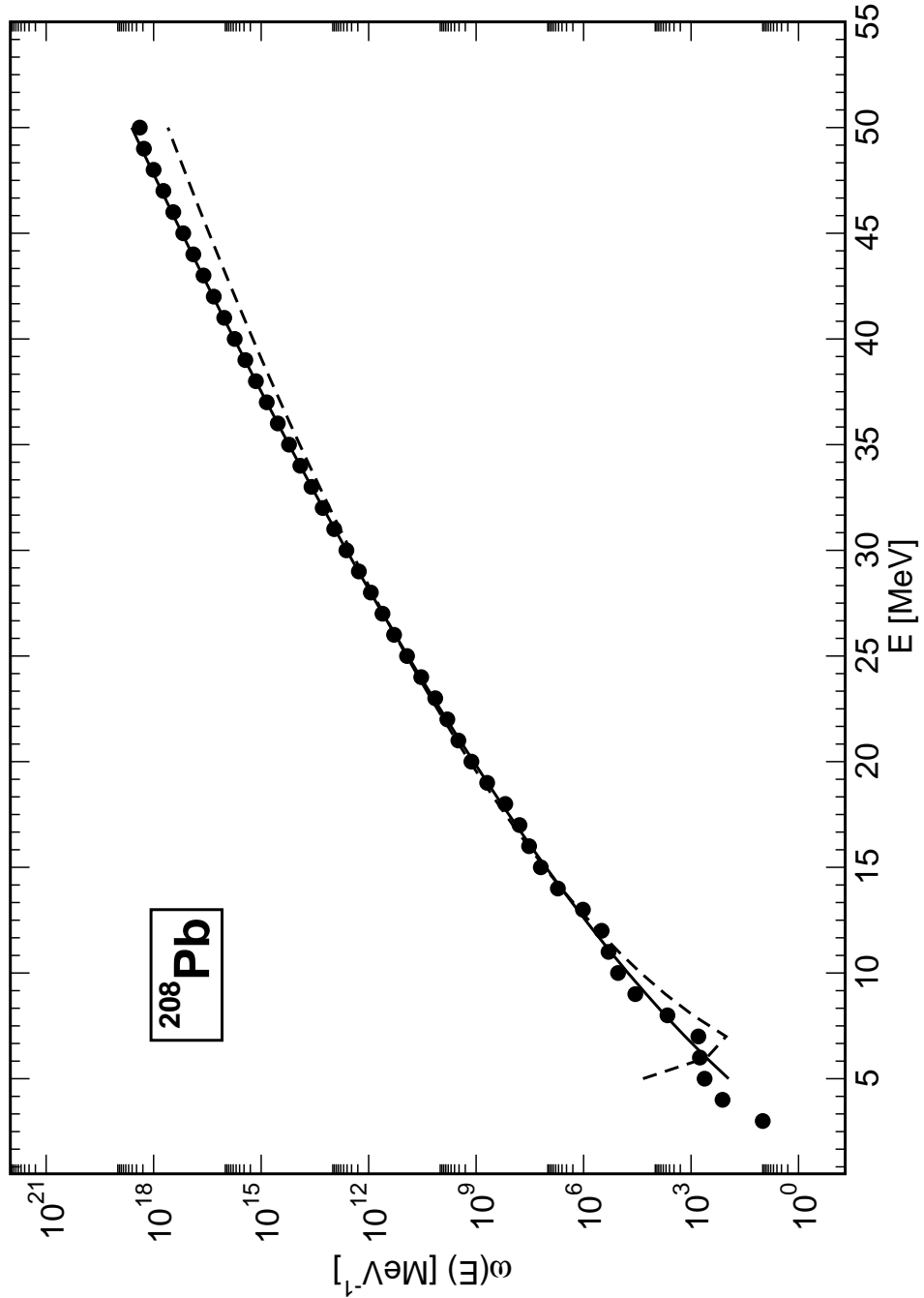


Fig. 4. Total state density of ^{208}Pb computed with the SPINDIS algorithm (dots) and fitted by BBF (27) (dotted line) and GBF (28) (solid line) in the [5,30] MeV interval. The BBF and GBF curves are extrapolated to the higher energy region for the sake of comparison with SPINDIS.

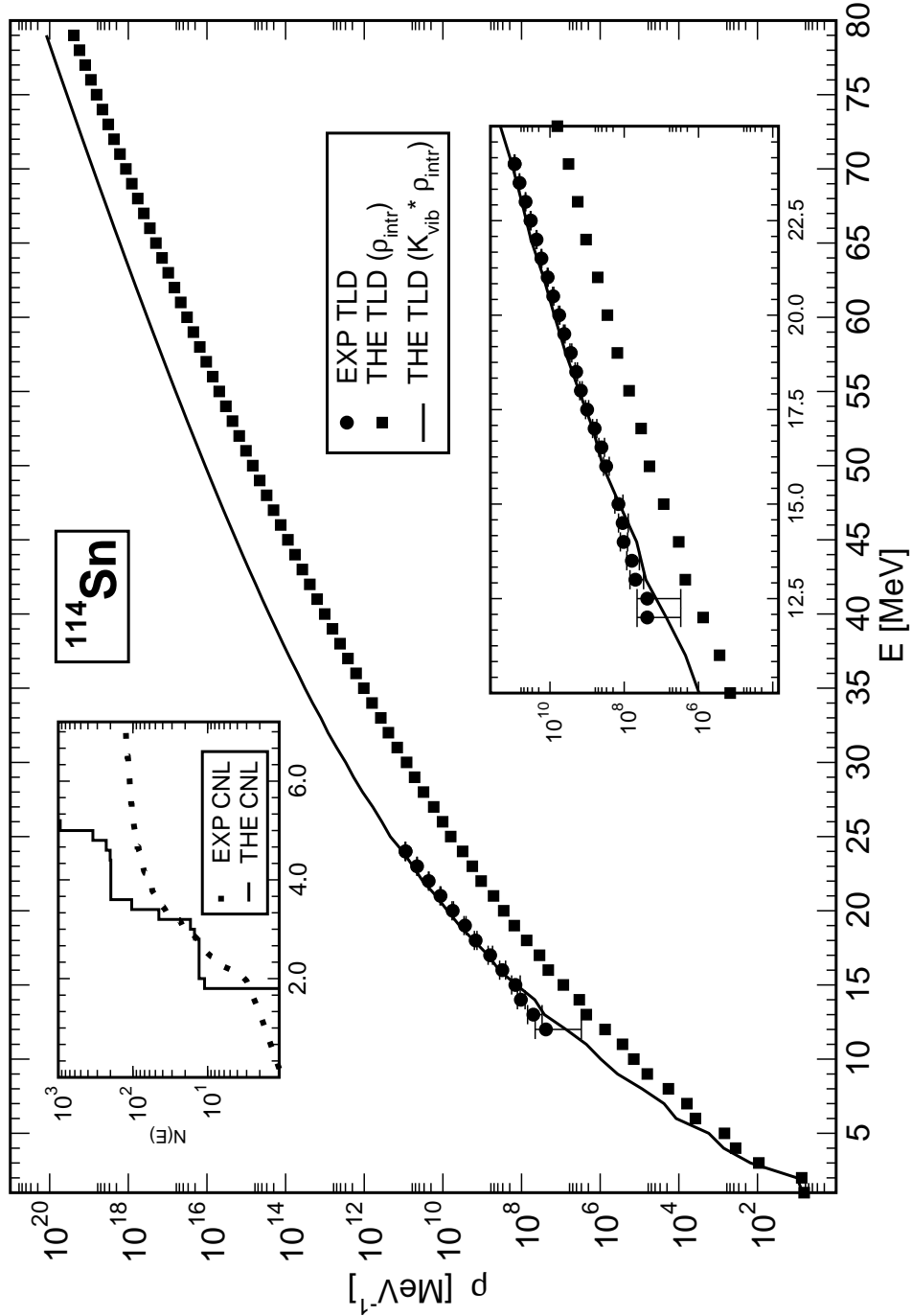


Fig. 5. Total level density (TLD) of ^{114}Sn as function of the excitation energy, calculated with (solid line) and without the vibrational enhancement factor (squares), and compared with experimental data from Ref. [44]. Lower right inset: the same results magnified with all available experimental points present. In the upper inset the calculated cumulative numbers of discrete levels (CNL) (solid line) are shown in comparison with the experimental values [43].

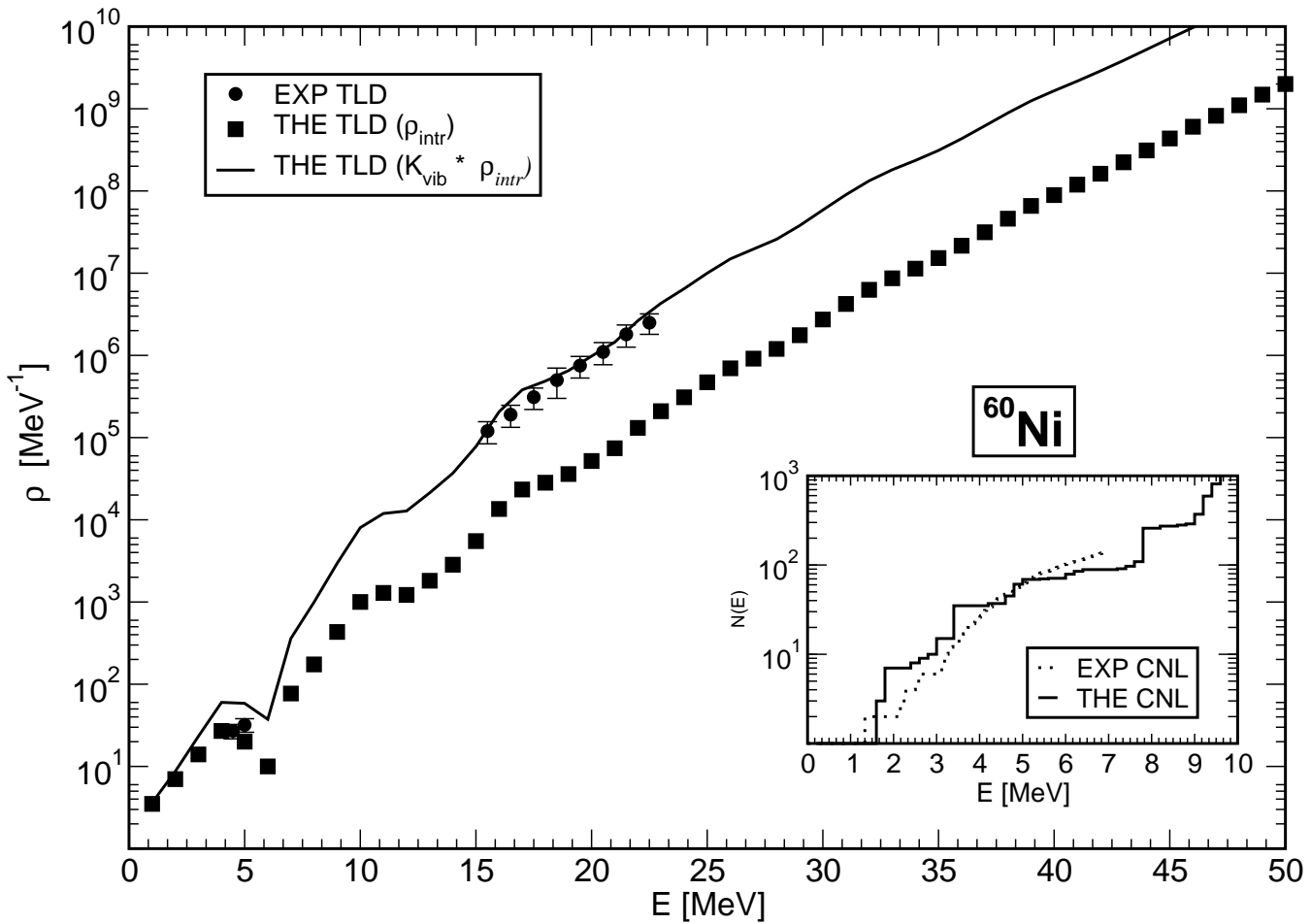


Fig. 6. The same as in Fig. 5, but for ^{60}Ni . The experimental data for the level density are from Ref. [45].

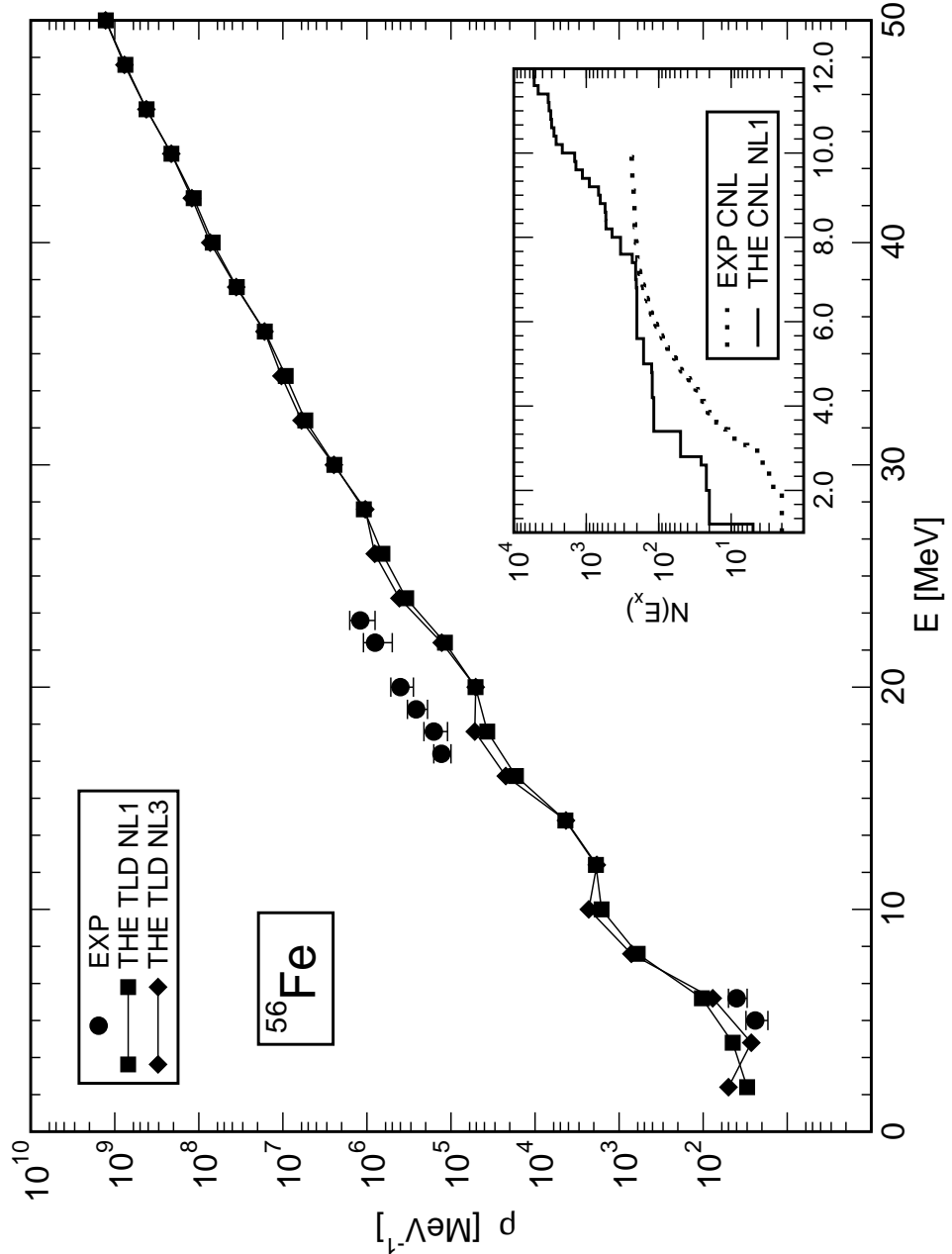


Fig. 7. Level densities of ^{56}Fe as functions of the excitation energy: a) The experimental data for the level density are from Ref. [51,45] (circles). b) total level density (TLD) calculated using NL1 parametrisation (squares); c) total level density (TLD) calculated using NL3 parametrisation (diamonds); In the inset the calculated cumulative numbers of discrete levels (CNL) (solid line) are shown in comparison with the experimental values [43].

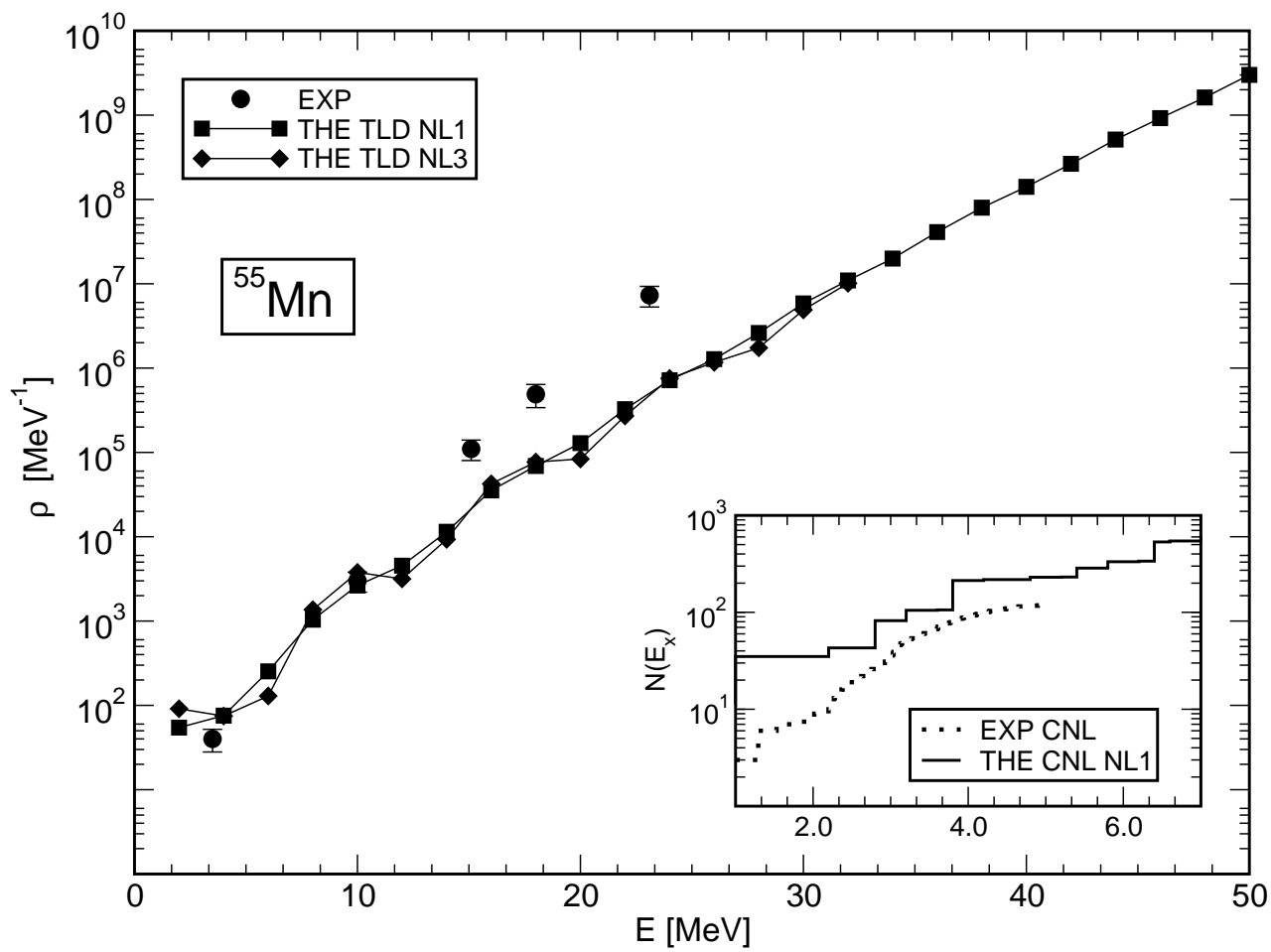


Fig. 8. The same as in Fig. 7, but for ^{55}Mn .